Optical Simulation and Colloidal Lithography Fabrication of Aluminum Metasurfaces

by

Chuyun Guan

A Thesis Presented in Partial Fulfillment
of the Requirements for the Degree
Master of Science

Approved May 2019 by the
Graduate Supervisory Committee:

Liping Wang, Chair
Bruno Azeredo
Robert Wang

ARIZONA STATE UNIVERSITY

August 2019

ABSTRACT

Solar energy has become one of the most popular renewable energy in human's life because of its abundance and environment friendliness. To achieve high solar energy conversion efficiency, it usually requires surfaces to absorb selectivity within one spectral range of interest and reflect strongly over the rest of the spectrum. An economic method is always desired to fabricate spectrally selective surfaces with improved energy conversion efficiency. Colloidal lithography is a recently emerged way of nanofabrication, which has advantages of low-cost and easy operation.

In this thesis, aluminum metasurface structures are proposed based on colloidal lithography method. High Frequency Structure Simulator is used to numerically study optical properties and design the aluminum metasurfaces with selective absorption. Simulation results show that proposed aluminum metasurface structure on aluminum oxide thin film and aluminum substrate has a major reflectance dip, whose wavelength is tunable within the near-infrared and visible spectrum with metasurface size. As the metasurface is opaque due to aluminum film, it indicates strong wavelength-selective optical absorption, which is due to the magnetic resonance between the top metasurface and bottom Al film within the aluminum oxide layer.

The proposed sample is fabricated based on colloidal lithography method. Monolayer polystyrene particles of 500 nm are successfully prepared and transferred onto silicon substrate. Scanning electron microscope is used to check the surface topography. Aluminum thin film with 20-nm or 50-nm thickness is then deposited on the sample. After monolayer particles are removed, optical properties of samples are measured by micro-scale optical reflectance and transmittance microscope. Measured and simulated

reflectance of these samples do not have frequency selective properties and is not sensitive to defects. The next step is to fabricate the Al metasurface on Al_2O_3 and Al films to experimentally demonstrate the selective absorption predicted from the numerical simulation.

ACKNOWLEDGMENTS

First of all, I would like to express my deep and sincere gratitude to my advisor Dr. Liping Wang, for his expert advice and encouragement throughout the research. This thesis would not have been possible without the help, support, and patience of him. I would also like to offer my sincere appreciation to Dr. Robert Wang and Dr. Bruno Azeredo, who devoted their valuable time to serve as my committee member and provided valuable advice.

I would also like to thank my group members Rajagopal, Payam, Linshang, Qing, Sydney and Xiaoyan. I learned a lot during interacting with them not only academically but also on a personal level. I would especially thank Rajagopal for his help and support during my research.

Finally, I extremely grateful to my parents for their caring and love. They provide me with both financial and psychological support which give me courage to face the difficulty during the research.

TABLE OF CONTENTS

Page

LIST OF TABLES iv

LIST OF FIGURE........ v

CHAPTER

1 INTRODUCTION 1

1.1. Spectrally Selective Surface 1

1.2. Colloidal Lithography 1

1.3. Objectives 3

2 NUMERICAL DESIGN AND SIMULATION 5

2.1. Proposed Spectrally Selective Surface 5

2.2. Numerical Method and Simulation Processes 5

2.2.1 Structure model 6

2.2.2 Material properties 7

2.2.3 Boundary condition 8

2.2.4 Analysis setup 10

2.2.5 Simulation convergence check 11

2.3 Results and Discussion for Metasurfaces on Al Substrate........ 13

3 SAMPLE FABRICATION........ 19

3.1. Substrate Cleaning 19

3.2 Self-assembly PS Monolayer Colloidal 19

3.3 Metal Deposition 21

3.4 Topography of PS Monolayer and Al Metasurfaces........ 22

4 OPTICAL PROPERTIES CHARACTERIZATION 25

4.1 Experimental Setup 25

4.2 Experiment Procedure 26

4.3 Reflectance of Undoped Silicon 27

4.4 Reflectance of the Fabricated Metasurface Sample 28

5 CONCLUSION AND FUTURE WORK 34

REFERENCES 35

CHAPTER 1

INTRODUCTION

1.1 Spectrally Selective Surface

Every object with none 0 K temperature participates in heat transfer with others at different temperatures via three mechanisms: conduction, convection, and radiation. Sun has an effective blackbody temperature of 5777 K which contains a huge amount of energy [1]. Solar energy has become one of the most popular renewable energy in human's life because of its abundance and environment friendliness. The energy produced in the interior of the solar sphere must be transferred out to the surface and then be radiated into space [2]. It has attracted lots of attention on how to make use of solar energy.

Radiation properties include transmittance, absorptance, reflectance and emittance which are all wavelength dependent properties. Energy transfer efficiency usually requires surfaces, which are usually called as spectrally selective surfaces, to absorb energy over one spectral range and reflect strongly over the rest of the spectrum. Spectrally selective surfaces have many different applications, for example, solar heat collector, which converts solar energy to useful heat and requires surfaces have high absorptance in 0.3 to 3 μm and high reflectance at wavelength longer than 3 μm [3], shown in Fig. 1.1. Spectrally selective surfaces can be achieved by ways such as multilayer thin films and periodic 1D or 2D structures[4-5].

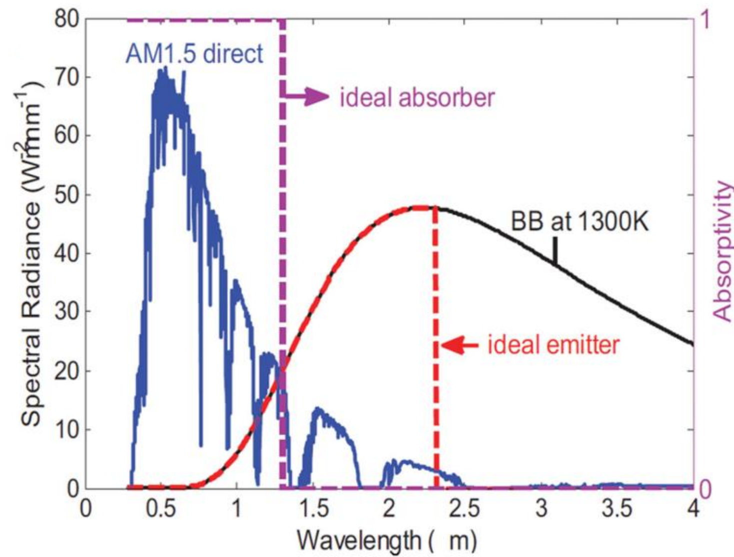

Figure 1.1. Spectral absorptivity of ideal absorber [6].

1.2 Colloidal Lithography

There are many ways to form periodic arrays of nanostructures over surface, such as photolithography, electron-beam lithography, electrochemical etching, and X-ray lithography. However, the actual implementation of these techniques can be very complex and expensive. Colloidal lithography (CL) is a recently emerged way of nanofabrication, which uses monolayer nanoparticles as masks for etching and deposition. The colloidal particles can be easily synthesized by conventional emulsion polymerization or sol-gel synthesis techniques and then self-assemble into two-dimensional colloid arrays [7].

There are several ways to self-assemble monolayer particles shown in Fig. 1.2 [8]. Fig. 1.2(a) is dip-coating in which capillary forces and evaporation induce colloidal self-organization. Lifting up a colloid array from an interface using the substrate is a more easily-controlled way shown in Fig. 1.2(b). This method can be combined with Langmuir-Blodgett film technique with which a large-scale monolayer of a colloidal array can be

obtained. Fig. 1.2(c) is electrophoretic deposition of colloids which drives the movement of the particles by applying electrical fields. Recent study of self-assemble methods has focused mostly on the enhancement of quality, controllability of the self-assembled structures. Fig. 1.2(d) and (e) are template-assisted self-assembly method. Fig. 1.2(f) shows the spin coating method.

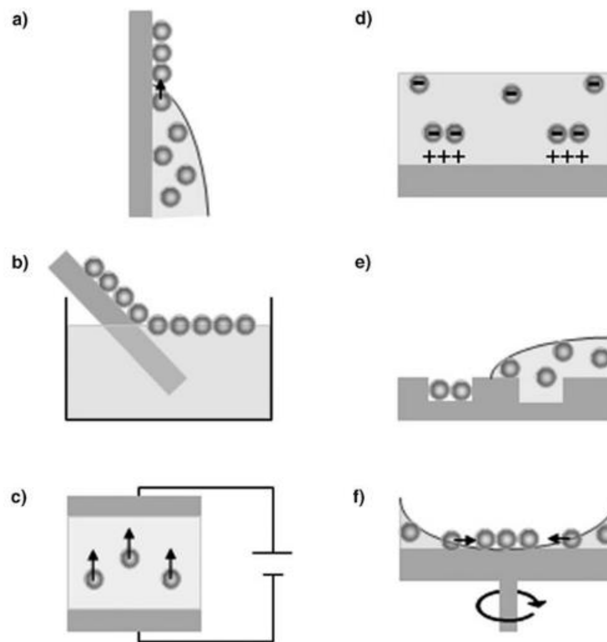

Figure 1.2. Diverse self-assembly strategies to create ordered colloid arrays: (a) dip-coating (b) lifting up a colloid array from an interface using the substrate (c) electrophoretic deposition of colloids (d) chemical or electrochemical deposition of colloids with a patterned array (e) physical template-guided self-organization of colloids (f) spin-coating [8].

Researchers can easily fabricate flexible and adoptable masks for growing diverse nanostructures. Compared to other nanostructure fabrication techniques, CL has advantages of low cost and easy operation. Recent research works have extended from the new assembly method and mechanism study to complex structures prepared by controlled assembly and optical applications of colloidal crystals [9]. Edward *et al.* created periodic

aluminum disk array that appears tunable absorption peak [10]. Bonakdar *et al.* created ring and crescent nanopillars that realized selective absorbers operating in the mid-infrared region of the spectrum[11]. Multiple structure can be created by flexible using the monolayer sphere. However, more potential structure can fabricate and there are still few studies on the optical properties of structures fabricated by CL.

1.3 Objectives

In this research, it is aimed to design a spectrally selective surface structure combined with CL method. The thesis is organized as follows; Chapter 2 uses High Frequency Structure Simulator to numerically study the optical properties and design metasurface structures to be fabricated by CL method. Chapter 3 focuses on the fabrication of monolayer mask by CL to check the feasibility of fabrication proposed structure. Chapter 4 presents the optical measurement of fabricated samples. The final chapter is a summary as well as a discussion of improvement and further studies regarding this research.

CHAPTER 2

NUMERICAL DESIGN AND SIMULATION

2.1 Proposed Spectrally Selective Surface

One proposed simple structure is by making use of the spacing between contacted spherical particles to create metasurfaces from metal deposition with the particles as masks. The top view of this structure is shown in Fig. 2.1. The unit cell of this metasurface structure will be like a bowtie-shaped structure within a parallelogram. By colloidal lithography, a hexagonal structure can be formed. The structure is designed to be Al metasurface on the top of aluminum or silicon substrate.

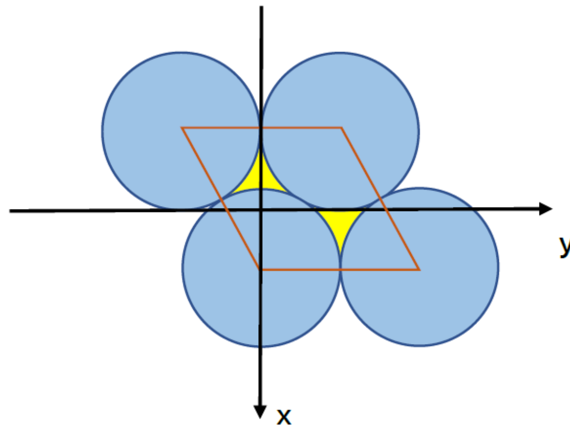

Fig. 2.1 Top view of the coordinate system for proposed structure.

2.2 Numerical Method and Simulation Processes

High Frequency Structure Simulator (HFSS) is a high-performance full-wave electromagnetic field simulator which integrates simulation, visualization, and solid modeling. HFSS can be used to calculate the optical properties of spectrally selective surfaces such as S-parameters, resonant frequency, and electromagnetic fields [7].

2.2.1 Structural model

One simple structure made of Al metasurface on Si substrate is used here to illustrate the simulation process. The first step of HFSS simulation is to build simulation structure. The 3D model will contain Si substrate, Al metasurfaces, and two air boxes, with one on the top and another on the bottom shown in Fig. 2.2. First, the default dimension unit is selected to "µm". Four circles with radius 0.25µm were drawn using the 2D draw tool. By selecting "properties" of each circle to enter their center positions and connect these four centers to create a polyline. The position for four circles is (-0.25, -0.25, 0), (-0.25, 0.25, 0), $(0.5 \times \frac{\sqrt{3}}{2} - 0.25,\ 0,\ 0)$, $(0.5 \times \frac{\sqrt{3}}{2} - 0.25,\ 0.5,\ 0)$. The thickness of Al metasurface is set to 50nm which can be drawn by doing "thickness" option for all surfaces just created and then "Boolean" operation for these objects.

The height of Si substrate is set to be 3000 nm. Although in fact, the silicon has a thickness around 5000 nm, it will not influence the result much to simplify the simulation calculation process in this way. As the longest wavelength interested in this research is 1000 nm. The according penetration depth of Si can be calculated by Eq. (2.1) [8] which is around 2800 nm.

$$t = \frac{\lambda}{4\pi k} \tag{2.1}$$

By selecting polyline and doing the thickness operation with thickness -3, Si substrate can be created behind metasurface. The height of air box is set to satisfy the top surface of air box far enough away to the metasurfaces. By doing the thickness operation again with thickness 0.5, air box can be created.

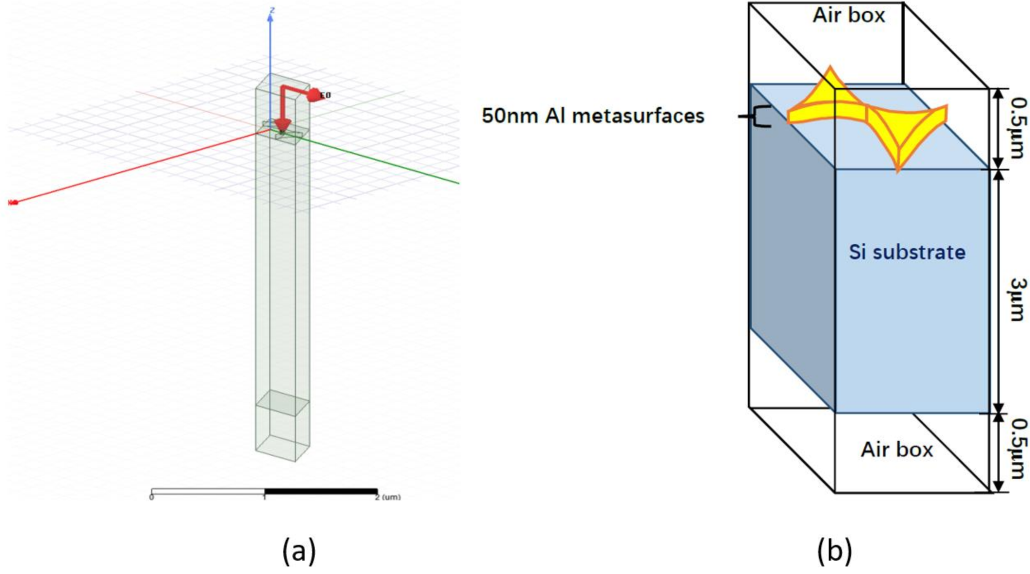

Fig. 2.2 3D model of the unit cell. (a) 3D model created in HFSS; (b) schematic of the structure.

2.2.2 Material properties

In ANSYS, the default materials properties are not frequency dependent. Users can import material relative permittivity and dielectric loss tangent by themselves. To get the reflectivity as a function of wavelength, the first step is to import material properties. From Handbook of Optical Constants of Solids [9], material refractive n and absorptive k at different wavelength can be found. According to the relationship between complex dielectric function ε and complex index of refraction m shown in Eq. (2.1) [10], the real and imaginary parts of the dielectric function can be easily written as Eq. (2.2) and Eq. (2.3), where ε' is the relative permittivity, and $\frac{\varepsilon''}{\varepsilon'}$ is the dielectric loss tangent.

$$\varepsilon = \varepsilon' - i\varepsilon'' = m^2 = (\mathrm{n} - \mathrm{ik})^2 \quad (2.1)$$

$$\text{where } \varepsilon' = n^2 - k^2 \quad (2.2)$$

$$\text{and } \varepsilon'' = 2nk \quad (2.3)$$

MATLAB is used to convert all the n and k data at wavelength range from 400 nm to 1000 nm to ε' and ε'' as a function of frequency, which are imported into HFSS as frequency-dependent optical properties for Si and Al. To make it easy to compare, these properties are plotted as a function of wavelength as shown in Fig. 2.3.

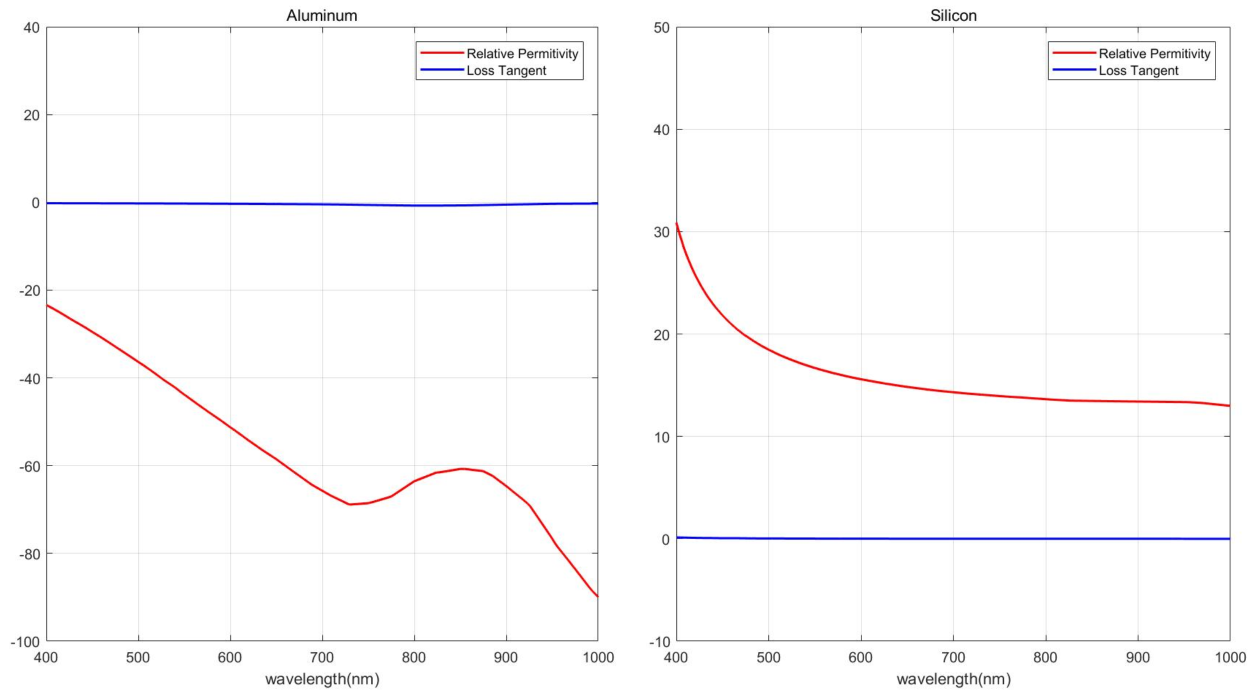

Fig. 2.3 Material properties as a function of wavelength (a) Al (b) Silicon.

2.2.3 Boundary conditions

Several boundary conditions are provided by ANSYS. Master and slave boundaries are useful for simulating periodic arrays. As this is a unit cell for a repeating structure, the boundary condition for side surfaces can be set to three pairs of master and slave for front and back surfaces and other three pairs of master and slave for left and right surfaces, shown in Fig. 2.4. Master/slave boundary assures that the electric field at each point on the

slave boundary matches that on the master boundary within a phase difference at each corresponding point. Here, the phase difference is set to be zero as only normal incidence is considered. By clicking the front surface of air box and clicking “Assign Boundary”, a master boundary is created. The coordinate system is created by adding a new vector at the position shown as Fig. 2.4 (a). Then slave boundary is assigned for the back surface in the same way. Only one additional option is to choose the corresponding master boundary which is “Master1” here. This procedure is repeated for six times to add all the boundary conditions for side surfaces shown in Fig. 2.4.

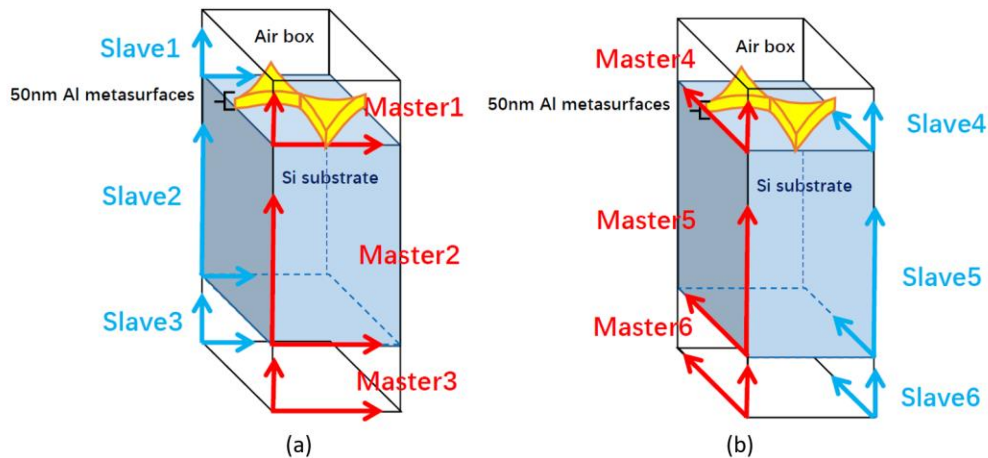

Fig. 2.4 Master/salve boundary condition: (a) for the front and back surface of air boxes and Si substrate; (b) for the right and left surface of air boxes and Si substrate.

The top and bottom surfaces for the air box have radiation boundary conditions shown in Fig. 2.5. Radiation boundaries work as absorbing boundaries which can model the surface as electrically open. Waves can radiate out of the structure and toward the radiation boundary. For frequency selective surface, by clicking “Reference for FSS”, HFSS will solve for the S-parameters which give information used in finding the optical properties of the structure.

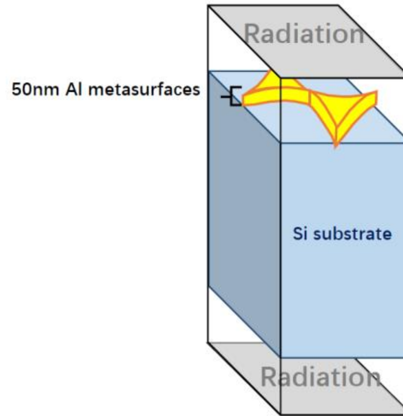

Fig. 2.5 Boundary conditions for the top and bottom.

The actual location of Cartesian system in simulation is shown in Fig.2.2(a). Wave port location in HFSS is always recommended on the surfaces exposed to the background. According to the simple geometry relationship, calculate the coordinates of excitation port to set it at the middle of top surface of air box with k_0 toward -z direction shown in Fig. 2.6.

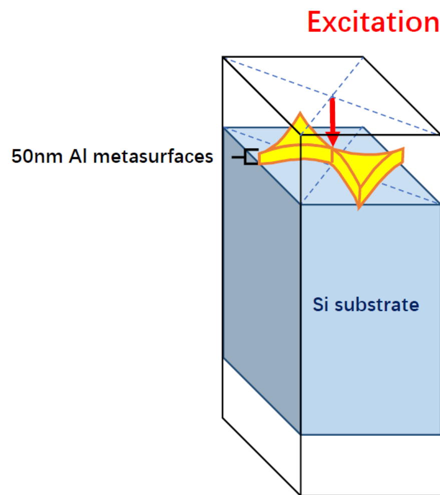

Fig. 2.6 Excitation port location.

2.2.4 Analysis setup

Solution type defines the type of results. Driven Modal which calculates the modal-based S-parameters is used in the simulation. The results for this solution type can be shown

in S-matrix which is expressed in terms of the incident and reflected waves.

First, solution setup is added by right clicking on “Analysis” in HFSS model tree. Solution frequency is used by adaptive mesher to automatically refine the mesh to electrical performance of the structure. Solution frequency is set to be at around the midpoint of the frequency sweep. The adaptive solutions option is used to define convergence criteria. HFSS uses adaptive meshing which will first setup an initial mesh, solves the fields, and then re-meshes based on where the fields have a high concentration and/or gradient. Each re-meshing step is defined as “adaptive pass”. “Maximum number of passes” controls the maximum times of re-meshing step will perform as it attempts to satisfy the convergence criteria. At each step, the scattering parameters are evaluated at each port and compared to the previous step. The difference between the two is defined as “delta S” [7]. Here, “Maximum number of passes” and “Maximum Delta S Per Pass” is set to be the default value 6 and 0.02.

Frequency sweep is added by right clicking the solution setup just created in HFSS model tree and clicking on “Add Frequency Sweep”. Choose “Discrete” under “Sweep Type”. This sweep type will perform a full solution at every frequency using the current mesh. Frequency range setting for the simulation should be consistent with effective experiment test range which is from 400 nm to 1000 nm in wavelength, or equivalently 300 THz to 750THz in frequency.

2.2.5 Simulation convergence check

Before running the project, one more step is to check the whole project by clicking the “Validate” bottom in the toolbar. After the simulation is done, a message will be shown

in the message window. By right clicking "solution setup" in HFSS model tree, convergence can be checked here. If the result is not converged, it is necessary to adjust convergence criterion in the adaptive meshing setting.

After checking convergence, matrix data for all frequencies can be displayed in a window include "Mag" and "Phs" which is magnitude and phase. The results are then exported and copied from ".tab" file into an Excel file.

Building block for this structure can be simplified like Fig. 2.7, which is a base two-port network.

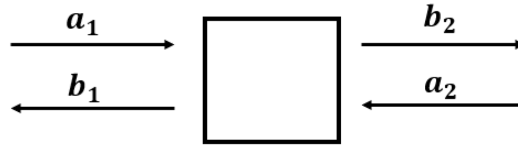

Fig. 2.7 Building block to calculate S parameter.

S-parameter matrix can be expressed as Eq (2.4) [8]. S[1, 1] is the reflection coefficient r of the structure. Then the reflectance can be calculated by Eq (2.5) [9]

$$\begin{pmatrix} b_1 \\ b_2 \end{pmatrix} = \begin{pmatrix} S[1,1] & S[1,2] \\ S[2,1] & S[2,2] \end{pmatrix} \begin{pmatrix} a_1 \\ a_2 \end{pmatrix} \quad (2.4)$$

$$\mathrm{R} = r^2 = S[1,1]^2 \quad (2.5)$$

To verify if the model is valid, A simple structure is created by changing the Al metasurfaces to an Al thin film with the same thickness 50 nm. Theory Al reflectance and simulation result is plotted in Fig. 2.8. The average deviation is less than 2%.

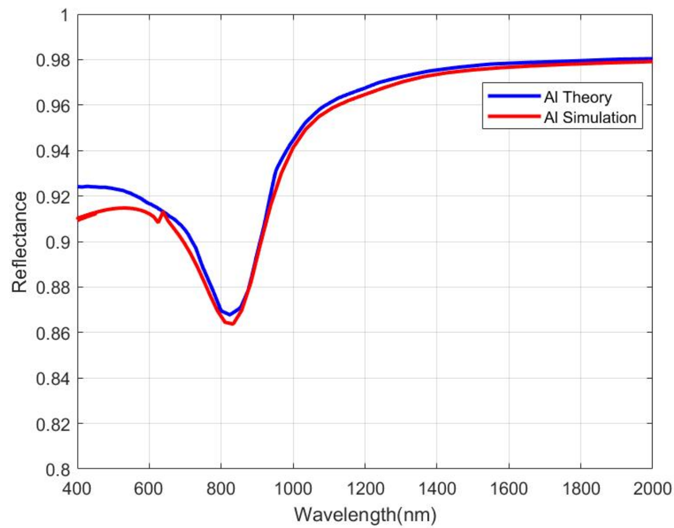

Fig. 2.8 Theoretical and simulated reflectance of 50 nm Al thin film.

2.3 Results and Discussion for Metasurfaces on Al Substrate

Another structure is designed with bowtie-shape Al metasurface on the Al substrate with and without Al_2O_3 film in between. Parameters of the structure with Al_2O_3 film is shown in Fig. 2.9(a), while Fig. 2.9(b) is the created model in HFSS.

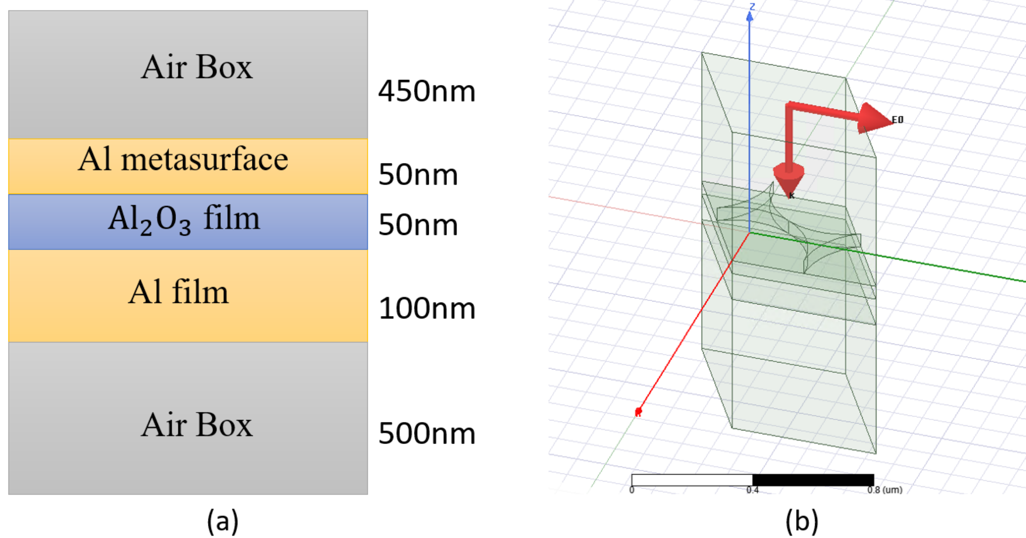

Fig. 2.9 Al metasurface on Al substrate with Al_2O_3 film in between: (a) thickness for each layer, (b) 3-D model created in HFSS.

As in the actual fabrication process, apex of bowtie shape antenna can hardly achieve point connection, another parameter, scale index, is introduced in the simulation. This parameter is used to simulate the situation where there is a gap between antennas. A smaller scale index indicates a smaller size of antenna and a larger gap between antennas. For example, scale 0.9 means that x and y dimension of metasurface is reduced to 0.9 times of its original. In this way, scale 1 is the original shape of metasurfaces. Fig. 2.10 is the top view of metasurface with scale index 1 and 0.9.

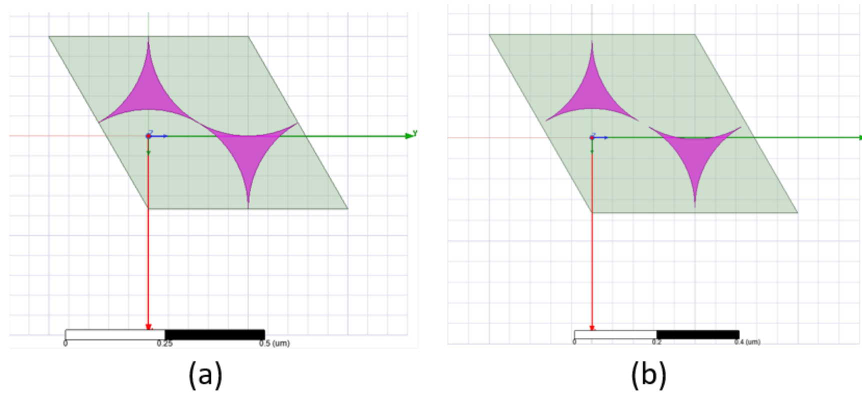

Fig. 2.10 Top view of metasurface with scale index of (a) 1 and (b) 0.9.

From Fig. 2.11, Coordinates of antenna centers C_1 and C_2 are $(-(\frac{d}{2}(1 - tan30°), 0)$ and $(\frac{d}{2}(2\cos 30° - 1 - tan30°), \frac{d}{2})$. The distance of two metasurface centers x then can be expressed as a function of particle diameter d, shown in Eq (2.6). In the case d = 500 nm, x is equal to 0.2887 μm and the width of the gap can be calculated by Eq (2.7). In the case scale index equal to 0.9, the gap width is equal to 0.02887 μm.

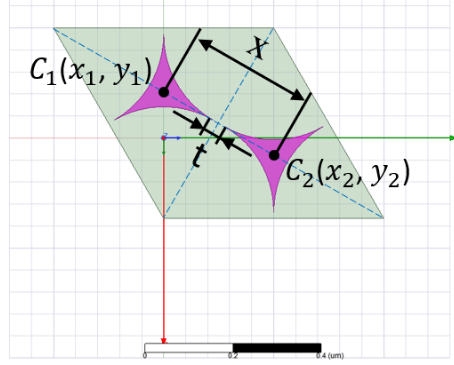

Fig. 2.11 Schematic of antenna centers' distance and gap width.

$$x = \sqrt{[-(\frac{d}{2}(1 - tan30°) - (\frac{d}{2}(2\cos30° - 1 - tan30°)]^2 + (\frac{d}{2})^2} \approx 0.5774d \quad (2.6)$$

$$t = x \times (1 - \text{scale index}) \quad (2.7)$$

The simulation set up is the same as the setting in metasurface on Si substrate. The reflectance of metasurface at different scale index with and without Al_2O_3 film is shown in Fig. 2.12.

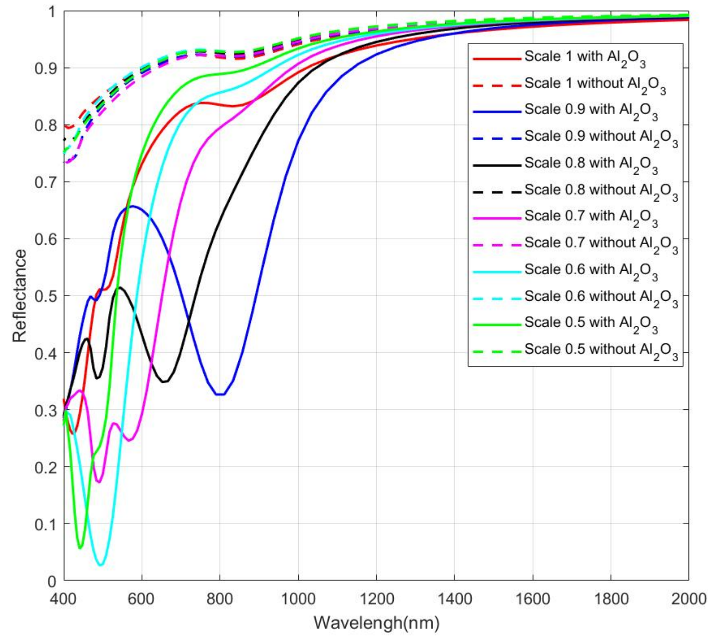

Fig. 2.12 Simulated spectral reflectance of Al metasurfaces at different scale index with and without Al_2O_3 film.

From the figure, spectral reflectance of Al metasurface structures without Al_2O_3

film have no obvious difference with different scale index, which are highly reflective. When 50-nm Al_2O_3 film is added between the Al metasurface and Al film, the spectral reflectance exhibits different and interesting features. With scale index = 1 (no gap between the antennas), the spectral reflectance becomes very low at short wavelengths, in particular around 500 nm. Note that the Al metasurface has a periodicity of 500 nm, and with Al_2O_3 layer, grating-coupled surface plasmon polariton could occur around 500 nm wavelength, which is responsible for the reduced reflection, or enhanced absorption around this short-wavelength region.

Furthermore, when the scale index is changed to 0.9, in which case, there is a gap between the antennas, a major reflectance dip around 800 nm wavelengths appears, indicating strong selective optical absorption. Interestingly, when the scale index decreases, or the gap increases, the reflectance dip shifts towards short wavelengths, suggesting tunable absorption peaks with different metasurface sizes and gap distance. When scale index is equal to 0.5, two reflectance dip overlaps which result in a minimum reflectance less than 0.1.

To further understand the physical mechanism of this major reflectance dip, electric and magnetic fields at 810 nm wavelength are plotted for the Al metasurface with scale 0.9 and 50-nm Al_2O_3 (Fig. 2.13), for the one with scale 0.9 without Al_2O_3 (Fig. 2.14), for the one with scale 1 and 50-nm Al_2O_3 (Fig. 2.15), and for the one with scale 1 without Al2O3 (Fig. 2.16). E and H fields in the cases without Al_2O_3 layer are almost evenly distributed without any indication of resonance. With Al_2O_3 layer, E and H fields are significantly enhanced around the antenna apex. When a gap exists between two antenna, H field induces an electric current loop, which strongly confines optical energy between the top antennas

and bottom Al film, resulting in strong optical absorption. It can be seen that the selective absorption is due to the presences of both Al_2O_3 layer and gap between the antennas. This can be explained by the magnetic polarization (MP) effect with a strong H field confinement within the Al_2O_3 between top antenna and bottom Al film. When scale equals 1 and there is no gap between neighboring antennas, there is no MP resonance or absorption because there is no gap capacitance for the LC circuit. In conclusion, absorption peak occurs because of the resonant LC circuit with Al_2O_3 layer as capacitor and disconnected antennas as inductors.

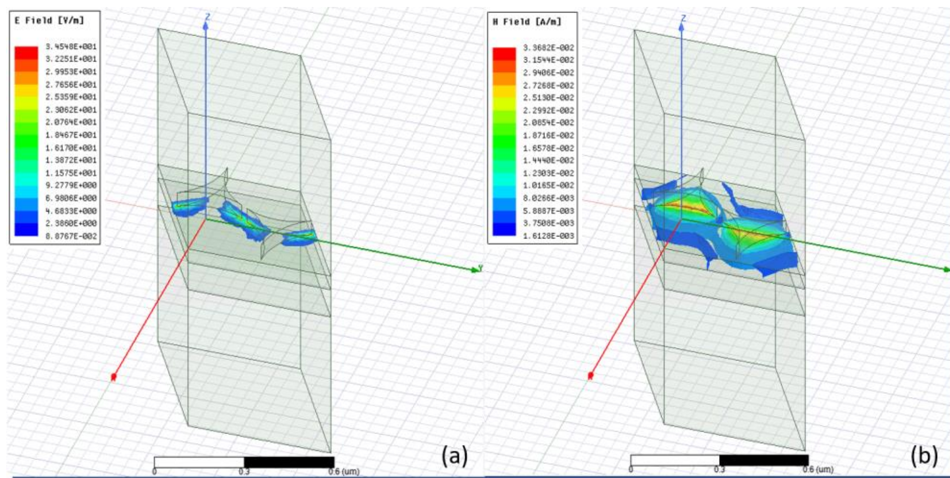

Fig. 2.13 Scale 0.9 with Al2O3 (a)E field (b) H field.

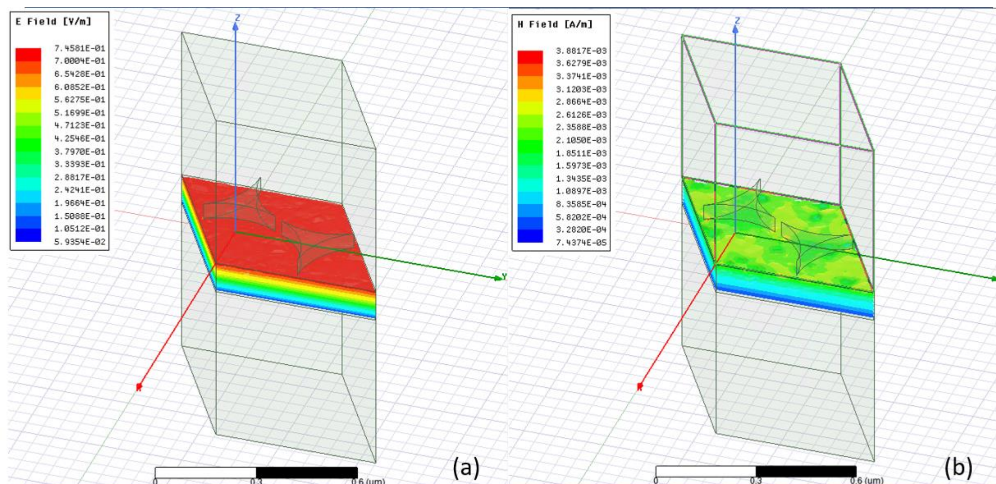

Fig. 2.14 Scale 0.9 without Al2O3 (a)E field (b) H field.

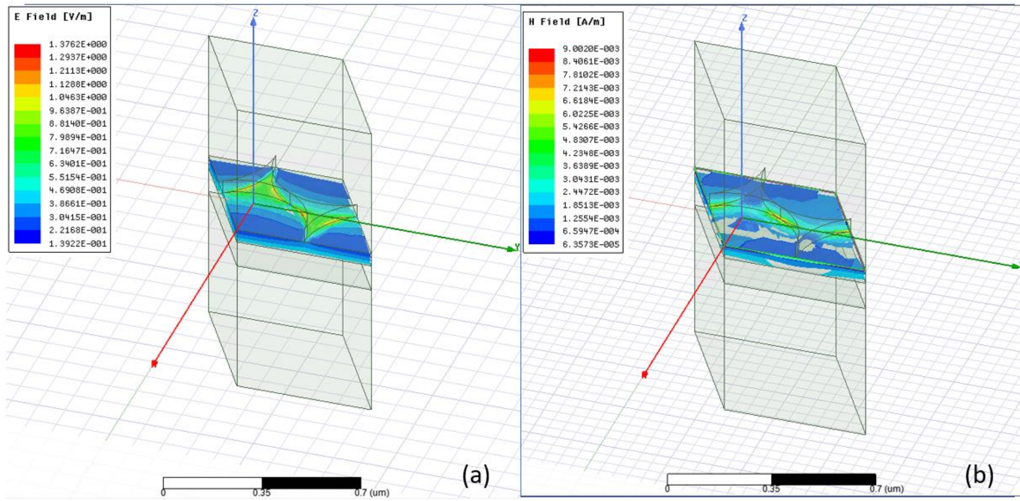

Fig. 2.15 Scale 1 with Al2O3 (a)E field (b) H field.

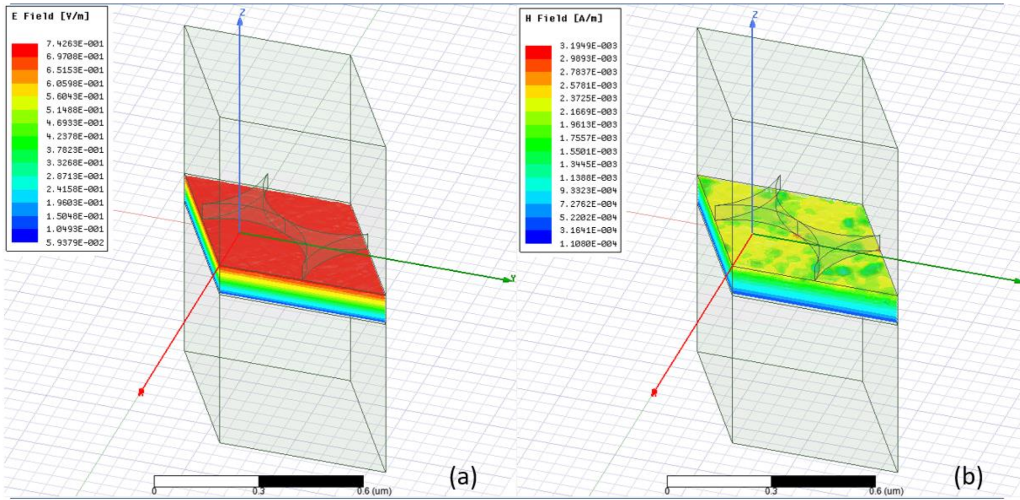

Fig. 2.16 Scale 1 without Al2O3 (a)E field (b) H field.

CHAPTER 3

SAMPLE FABRICATION

3.1. Substrate Cleaning

In this experiment, microscope glass slides, silicon substrate of two sizes are used: $0.5 \times 0.5\text{cm}$ silicon pieces and roughly $3 \times 2\text{cm}$ silicon pieces. Microscope glass slides are sonicated cleaned by acetone, methanol, and IPA successively and then dried with gentle air flow. Glass slide is used to lead the Polystyrene particles (PS) suspension to the air-water interface. This process is to not only relieve the dirty from the substrate but also make glass slide hydrophilic so that PS suspension can flow freely to the air-water surface. All silicon substrates are plasma cleaned which also play a role to make them hydrophilic.

3.2 Self-assembly of Monolayer PS Colloidal Particles

Polystyrene particles with a diameter of $500 \pm 100nm$ $5wt\%$ from Spherotech,Inc are used in the experiment. The first step is to dilute this PS suspension. PS suspension is shaken several times before using to make sure that particles dispersed uniform. Ethanol with purity $\geq 99.5\%$ is mixed with equal volume DI water. Then PS suspension is diluted in equal volumes of the mixed solvent of ethanol and DI water and then ultrasonicated 15 minutes for absolute uniformity. The final PS suspension has concentration of 2.5wt%. Diluted PS suspension is stored at fridge with temperature below 5°C. All the PS suspension used in the following experiment is the diluted 2.5wt% one. The suspension is ultrasonically dispersed at least 10 minutes each time before use. Sodium dodecyl sulfate (SDS) powder was purchased from Sigma-Aldrich. SDS powder is diluted in DI water to get a solution with a concentration of $2wt\%$. In this experiment, SDS

solution is used to modify surface tension so as to help PS particles form a monolayer. A Petri dish is filled with DI water. A glass slide is positioned at around 45° angle in the Petri dish. The larger silicon substrate can be positioned at around 30° angle in the Petri dish on the other side as shown in Fig 3.1(a).

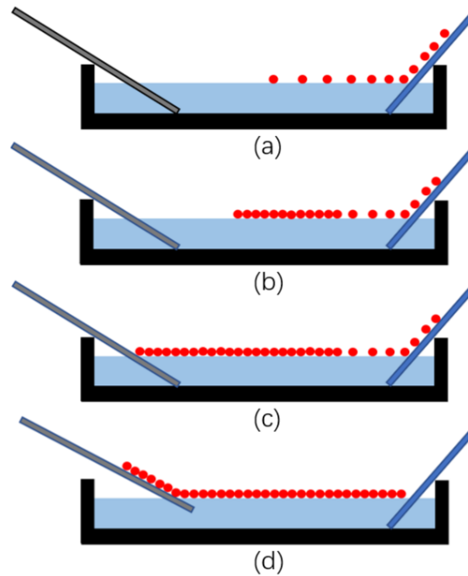

Fig. 3.1 Preparation PS monolayer on silicon substrate. (a) PS suspension pipetted onto an angled glass substrate and move onto air-water interface. (b) PS particles assembling on air-water interface. (c) As more suspension joins the monolayer, full coverage over the surface is obtained. (d) Lift substrate to transfer the monolayer.

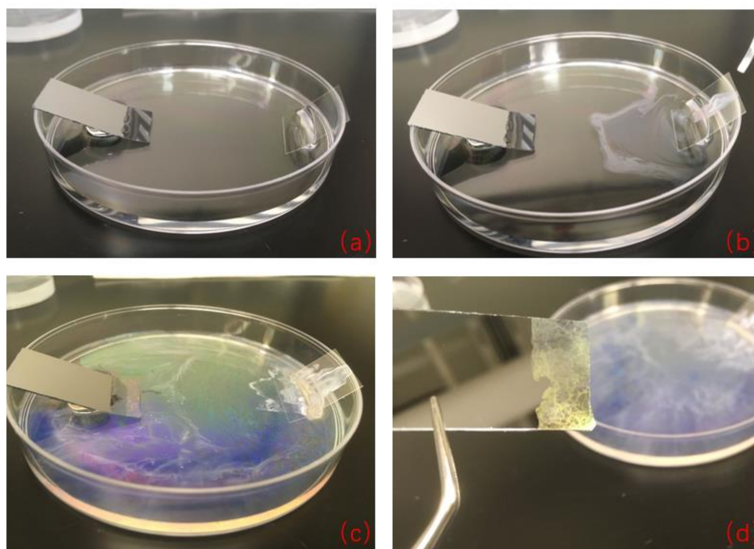

Fig. 3.2 Corresponding experiment procedures.

Then, one drop of SDS solution is added to the DI water. After 5 minutes, around 0.02ml diluted PS suspension is added. The most important point in this process is to avoid turbulence brought by adding PS suspension. Turbulence will change the surface tension of the water-air interface and break the force balance which will break the monolayer already formed and also influence the further formation of monolayer. In this experiment, PS suspension is pipetted onto the glass slide so that PS suspension will move freely along the slides into the water-air interface. In this step, the PS suspension is added slowly and each time only around 2μl suspension is pipetted. Once the prior drop completely diffused and there is no visible movement on the air-water interface identifiable by the naked eye, the suspension will continue be pipetted. After pipetting the suspension, the diffraction light can be seen once the monolayer is formed. Waiting for a few minutes to let the monolayer stable, slowly take off the larger silicon substrate and the monolayer will be transferred on silicon substrate. 0.5×0.5cm silicon pieces can slowly insert into the water by a tweezer at around 10° angle and then lift them up to transfer the PS monolayer.

3.3 Metal Deposition

Aluminum (Al) with a thickness of 50 nm is then deposited on the silicon substrate using PS monolayer as mask, shown in Fig. 3.3(a). After metal deposition, polystyrene particles are removed by keeping the wafer into acetone and methanol ultrasonic bath at 40℃ for 30 minutes successively. The particles are excepted to array in hexagon. After removing PS particles, the final metasurface looks like Fig. 3.3(c).

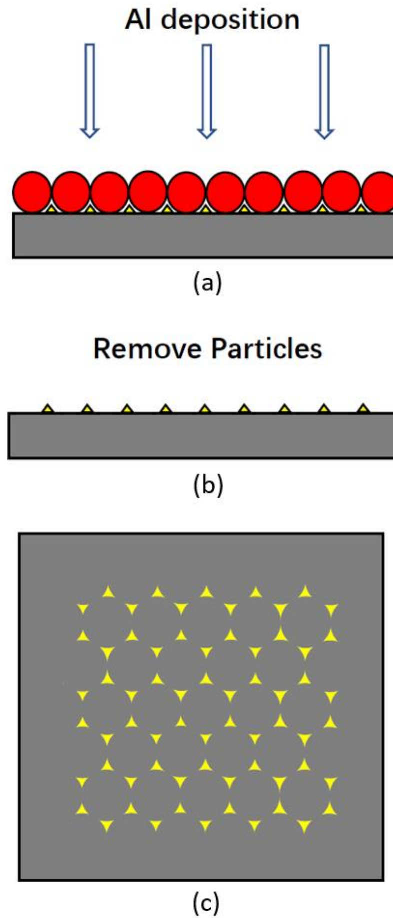

Fig. 3.3 Preparation Al metasurfaces on silicon substrate. (a) deposition Al using PS monolayer as mask (b) Removal of Particles (c)Top view of final structure.

3.4 Topography of PS Monolayer and Al Metasurfaces

In this research, optical microscope and scanning electron microscope (SEM) is used to observe the topography of PS monolayer and Al metasurfaces. Before metal deposition, it's important to know whether the particles are connecting one by one and only formed to one layer. As the maximum magnification of optical microscope is 1000 while the diameter of PS particles is about 500nm, it's hard to answer this question by optical microscope. To check it, SEM images were taken, shown in Fig. 3.4. At the edge of the sample Fig. 3.4(a), it can be seen clearly that PS particles only formed to one layer. At some point, there are particles integrate together to a group. However, in most area, the particles

contact one by one in a hexagonal shape.

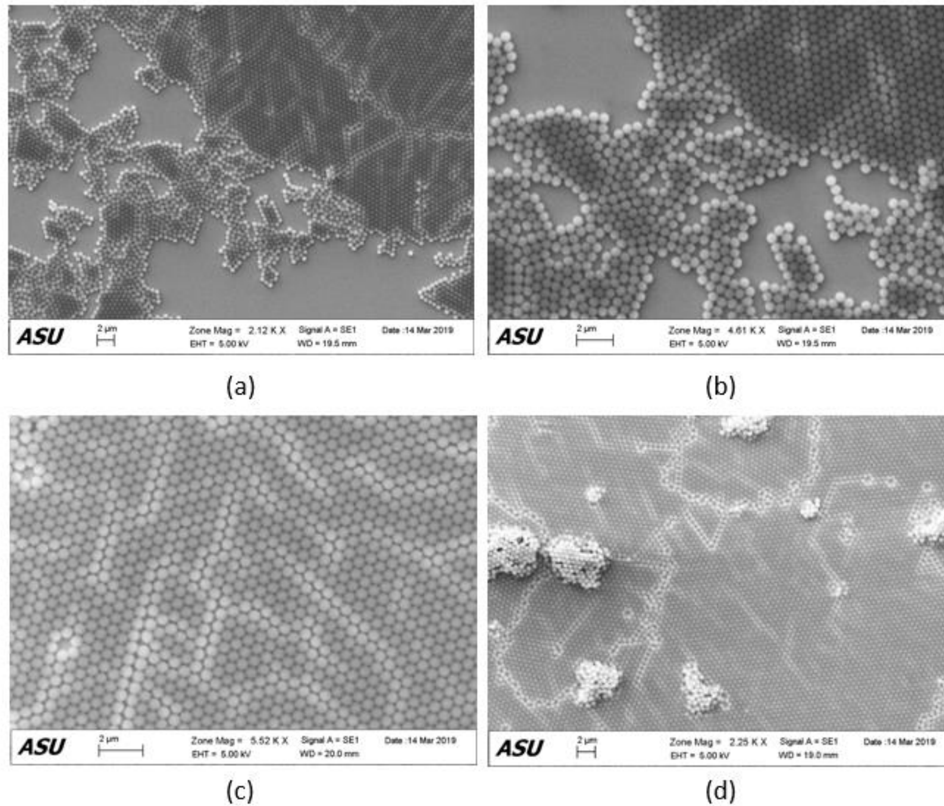

Fig. 3.4 SEM image of PS monolayer: (a) at the edge of the sample (b) zoom in (c) middle area of sample (d) integral PS particles group

After 50nm Al metal deposition， optical microscope is used to check the removal of PS particles. Fig. 3.5(a) is the image before removing particles with magnification 100. The purple area is PS particles with Al metal on top. Fig. 3.5 (b) is image after soaping sample in ultrasonic acetone and methanol to remove particles. The whole purple area changes to gray color which means all PS particles have been removed and the gray color should be Al metasurfaces.

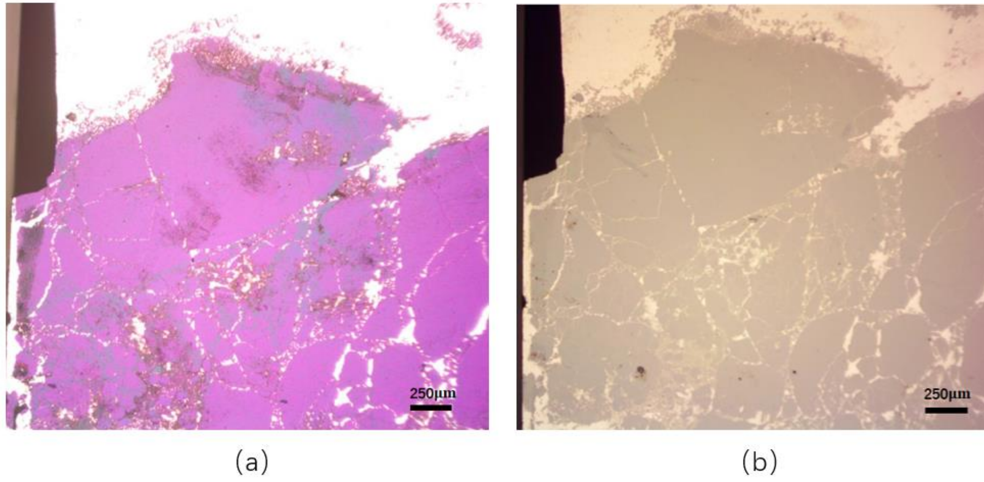

Fig. 3.5 Optical microscope image for sample after Al deposition (a) before and (b) after removing PS particles.

CHAPTER 4

OPTICAL PROPERTIES CHARACTERIZATION

4.1 Experimental Setup

The final step is to test the optical properties of fabricated sample. Micro-scale optical reflectance and transmittance microscope (MORT) is used to test optical properties in this research. Figure 4.1 shows the schematic of the setup. Tungsten lamp is the light source for the equipment. Optical cable carries the light to the collimator which will then sends the lights to a 50:50 beam splitter. This beam goes and gets reflected back from the sample, part of which goes to the camera and part to the spectrometer through the optical cable. From this equipment, we can gather intensity of reflected light source. By calculating intensity ratio between sample to be test and reference sample, we can get the reflectivity of the sample. Usually, Al is used as reference sample as it has high reflectance which will give small deviation when doing calculation.

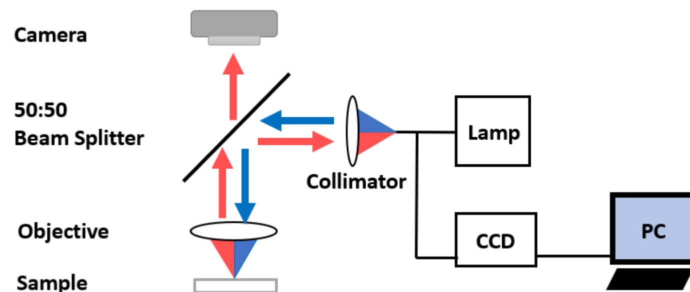

Fig. 4.1 Schematic MORT microscope

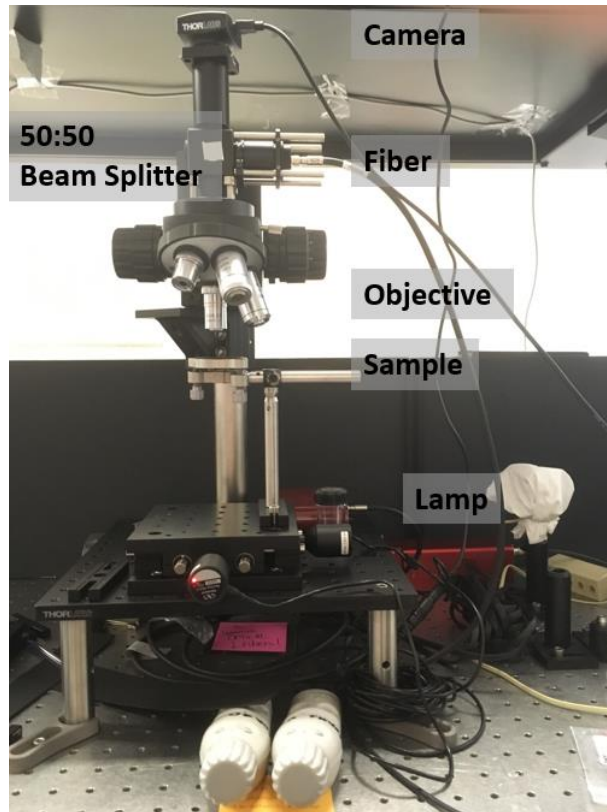

Fig. 4.2 Actual image of MORT microscope

4.2 Experiment Procedure

First, Al is tested as a reference sample. To make sure the light source is stable and the result is not affected by the environment a lot, test different positions of Al sample for at least 3 times. First, Al sample is placed on the sample holder. By modifying the actuators and stage tilt screws, the best focus can be got which is also the best signal amplitude seen from the spectrometer software. When the curves each time are basically coincident, the result is recorded as Al intensity as a function of wavelength. To validate our measurement technique, measuring reflectance of a undoped silicon wafer was needed. Next, follow the same steps to test intensity of sample with metasurfaces. Finally, calculation function can be used on the software to calculate the ratio between intensity of undoped silicon and Al,

sample with metasurfaces and Al separately. When wavelength is below 400 nm or exceeds 1000 nm, reflectance data is not accurate, as there is a large area fluctuation of the ratio. In this research, we only process the data with wavelength between 400 to 1000 nm. Relationship between measured intensity and reflectance can be expressed by Eq(4.1). Therefore, final reflectance of the sample can calculate by Eq (4.2).

$$I_{Sample} / I_{Al} = R_{Sample} / R_{Al} \tag{4.1}$$

$$\text{Therefore, } R_{Sample} = I_{Sample} / I_{Al} \times R_{Al} \tag{4.2}$$

4.3 Reflectance of Undoped Silicon

From Maxwell equation, the relation between reflectance and refractive index is shown in Eq (4.3), where n is refractive and k is absorptive index. These data can be found from Handbook of Optical Constants of Solids. Equation (4.3)[10] is used to calculate theoretical reflectance of Si.

$$R = \frac{(n-1)^2 + k^2}{(n+1)^2 + k^2} \tag{4.3}$$

Theoretical and measured reflectance of undoped Si were plotted in Fig. 4.3 shown below.

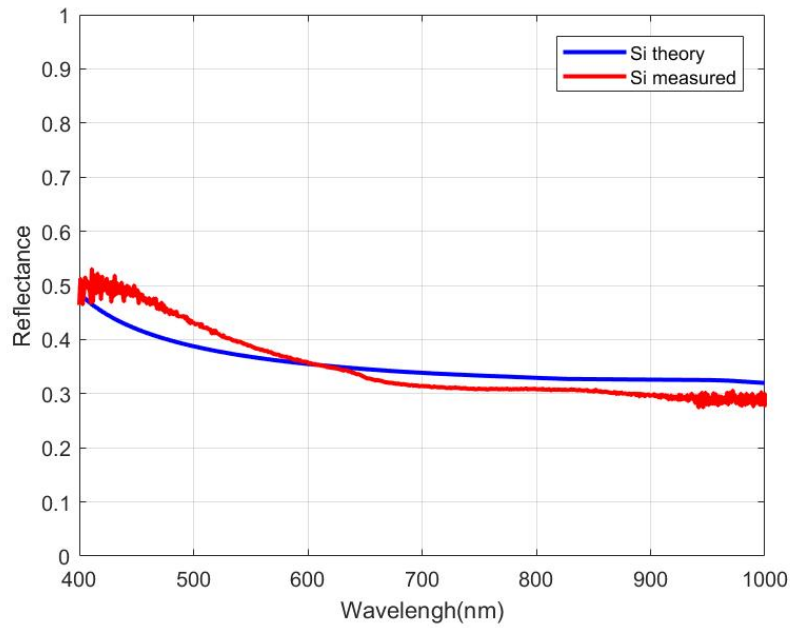

Fig. 4.3 Theoretical and measured reflectance of undoped Si as a function of wavelength

4.4 Reflectance of the Fabricated Metasurface Sample

Each sample is measured three times by changing the tested position. The optical image of test positions is shown in Fig. 4.4. The final structure is not that uniform with some dark points which is Al on top of unwashed out PS particles. The light area is Al metal as the substrate has some area uncovered monolayer mask.

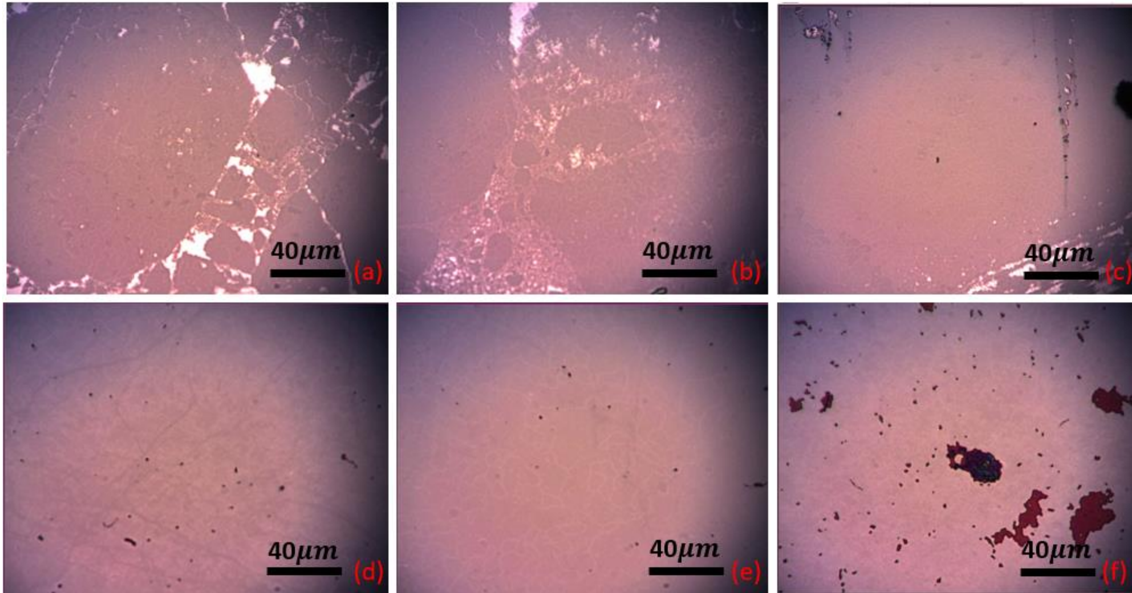

Fig. 4.4 Optical image of test positions of (a) 50nm-Al metasurfaces at position 1, (b) 50nm-Al metasurfaces at position 2, (c) 50nm-Al metasurfaces at position 3; (d) 20nm-Al metasurfaces at position 1; (e) 20nm-Al metasurfaces position 2; (f) 50nm-Al metasurfaces at position 3.

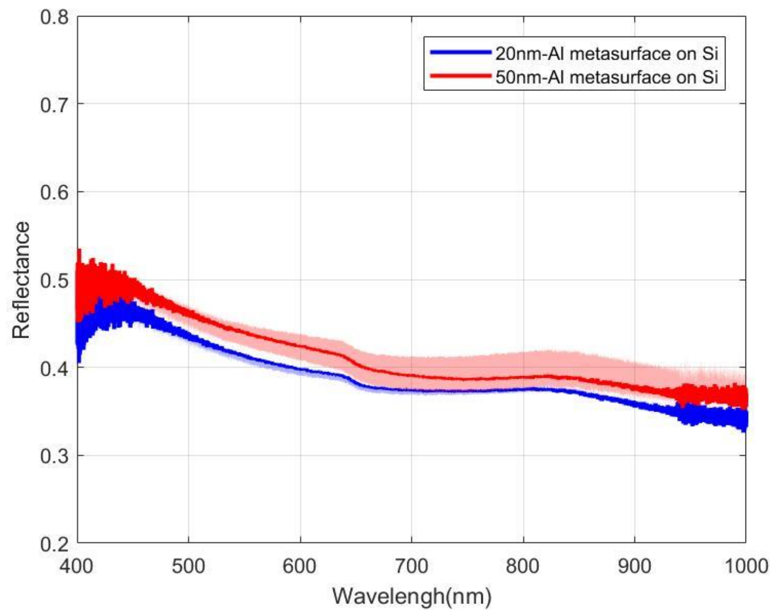

Fig. 4.5 Measured spectral reflectance of 50-nm and 20-nm Al metasurface on silicon as a function of wavelength.

The same Al reference sample is used to calculate intensity ratio. There are no spectral selective properties at this range of wavelength not as expected. Measurement

results for different test point do not have much variations. Average reflectance after calculation is plotted in Fig. 4.5, in which shaded area is the error bar. Reflectance for sample with 50nm Al metasurface at different position have more difference compared to 20nm metasurface sample. Reflectance of each tests is then plotted in Fig. 4.6. At position 1 and 2, relative more Al metal area exposed compared to position 3 which result in higher reflectance.

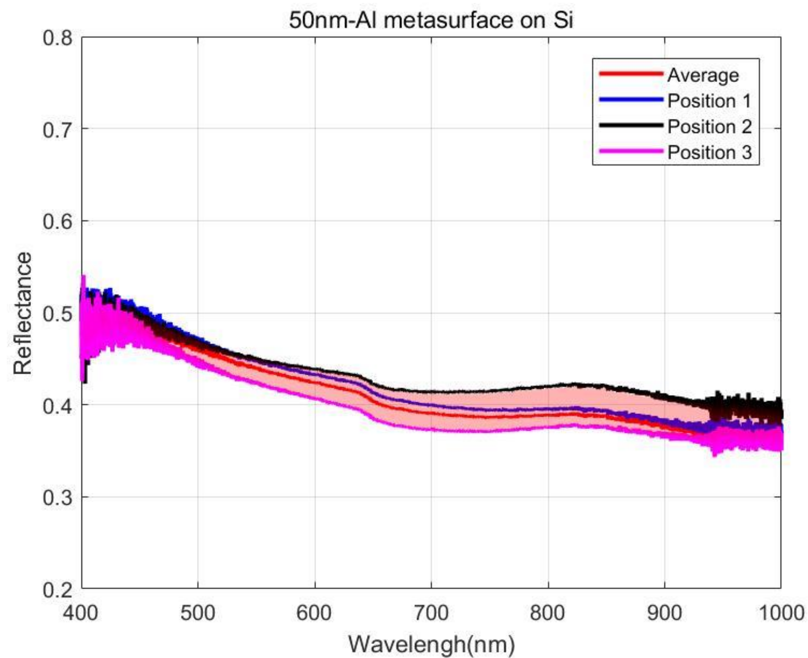

Fig. 4.6 Measured spectral reflectance of 50-nm Al metasurface on silicon as a function of wavelength.

However, reflectance of the samples do not have any selective properties and are nearly the same as the reflectance of undoped Silicon. Simulation is done here to help understand the measured reflectance. First, reflectance of silicon is simulated treating silicon as semi-infinite substrate which is then compared to theoretical reflectance shown in Fig 4.7. Simulated reflectance does not match the theoretical data perfectly but can be

accept within tolerance. Next, reflectance of the same structure with fabricated sample is simulated and plotted in Fig 4.8. From simulation results, reflectance of 50nm-Al and 20nm-Al metasurfaces is around 0.5 at all spectral range with 50nm metasurfaces structure a little higher than 20nm metasurfaces structure which is consistent to measured result.

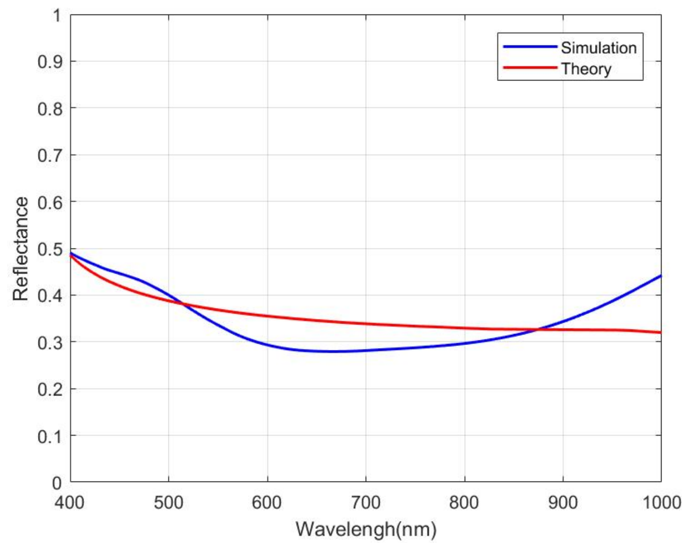

Fig. 4.7 Simulation and theory reflectance of Si film.

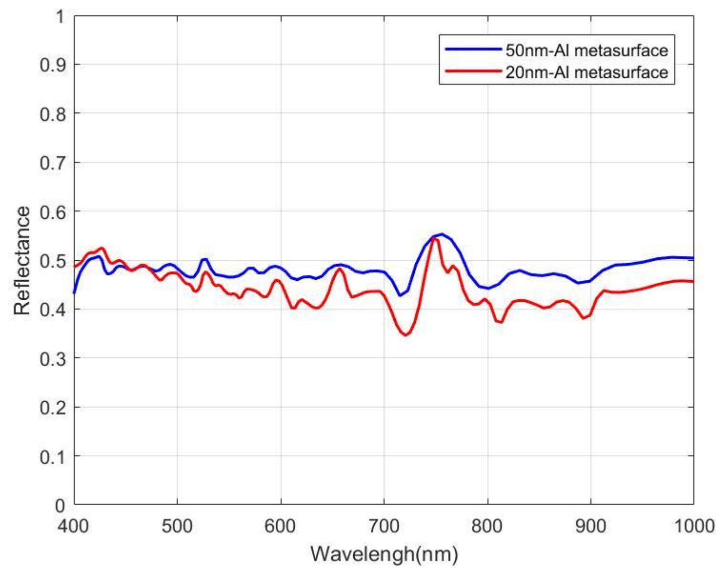

Fig. 4.8 Simulation reflectance of Al metasurfaces on Si substrate.

However, simulated reflectance has fluctuation. Considering actual sample has

defects which may affect the measured reflectance. Another model is created to simulate the situation when defects exist. Newly built structure contains six unit cells(showed in Chapter 2) and arrays in 2×3. To simulate defects, scale indexof one of the cells is set to 0.9 and one cell has no metasurface on it, shown in Fig. 4.9.

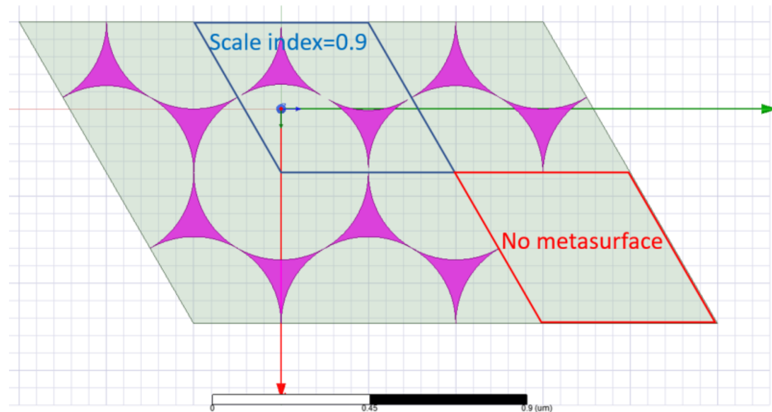

Fig. 4.9 Top view of simulated structure with defects.

In this case, structure is much complicated which makes it hard to converge. Several attempts are done here to correct the model such as adjust air box height, silicon substrate thickness, mesh size, and convergence criterion. However, it still does not gain a good result. One of simulation results is shown in Fig 4.9. Reflectance is still fluctuated at 0.5 but has much higher fluctuation compared to no defects case. This can explain why measured reflectance at different points has a few changes even topography has some difference. Defects can only change the fluctuation intensity and have limited influence to results.

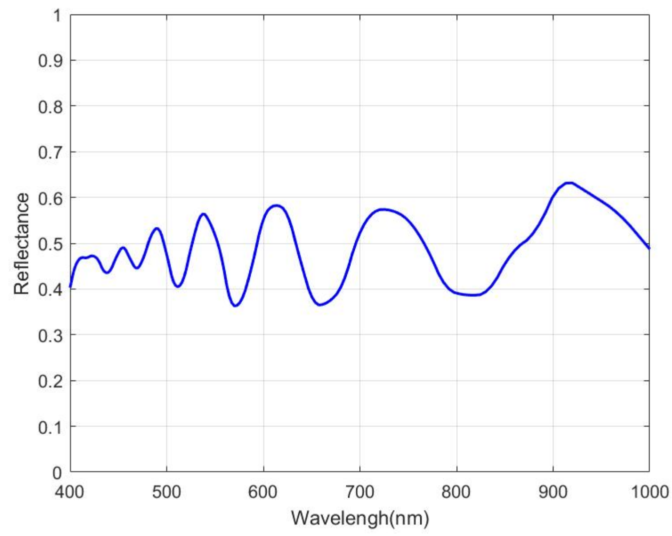

Fig. 4.9 Simulatied reflectance of 50nm-Al metasurfaces on Si substrate with defects.

CHAPTER 5

CONCLUSION AND FUTURE WORK

In this thesis, one kind of metasurfaces structure is proposed based on colloidal lithography method. High Frequency Structure Simulator is used to create the structure and simulate optical properties. Simulation model is checked valid by simulating aluminum thin film reflectance and compared with theory. Simulation results show Al metasurfaces on Al_2O_3 film on Al substrate has two relative reflectance dips with the smallest reflectance can reach less than 10%. As the metasurface is deposited on 100nm aluminum thin film, which is opaque, it indicates selective absorption up to 90% around these two wavelengths. Colloidal lithography is used to fabricate proposed sample physically. Monolayer PS mask is created successfully. The optical properties of sample are measured and compared with simulation result. Measurement is checked valid by test reflectance of undoped Si and compared with theory. However, measured reflectance of the samples does not have any selective properties as shown in simulation and are nearly the same as the reflectance of undoped silicon. Simulation explains that defects only has limited influence to reflectance.

The simulation model can be used to simulate more structure by simply modifying the thickness of Al or the dimension of bowtie-shape structure. For further improvement, the relationship between thickness of Al metasurfaces and optical properties can get by doing more simulation. SEM test is needed to further confirm the final geometry of fabricated sample. There are some challenges of fabricating sample with less or no defects and removing PS particles appropriately.

REFERENCES

[1] American Society for Testing and Materials. E490-00a (2006). ‘‘Standard Solar Constant and Zero Air Mass Solar Spectral Irradiance Tables.’’

[2] Deceased, J. A. D., & Beckman, W. A. (n.d.). *Solar Engineering of Thermal process*.

[3] Dimitrov, A. S., & Nagayama, K. (1996). Continuous Convective Assembling of Fine Particles into Two-Dimensional Arrays on Solid Surfaces. Langmuir, 12(5), 1303–1311. https://doi.org/10.1021/la9502251

[4] Rinnerbauer, V., Lenert, A., Bierman, D. M., Yeng, Y. X., Chan, W. R., Geil, R. D., … Wang, E. N. (2014). Metallic Photonic Crystal Absorber-Emitter for Effi cient Spectral Control in High-Temperature Solar Thermophotovoltaics, 1–10. https://doi.org/10.1002/aenm.201400334

[5] Wang, L. P., & Zhang, Z. M. (2017). Wavelength-selective and diffuse emitter enhanced by magnetic polaritons for thermophotovoltaics, 063902(December 2011), 2010–2013. https://doi.org/10.1063/1.3684874

[6] Auzelyte, V., Gallinet, B., Flauraud, V., Santschi, C., Dutta-gupta, S., Martin, O. J. F., & Brugger, J. (2013). Large-Area Gold / Parylene Plasmonic Nanostructures Fabricated by Direct Nanocutting, 50–54. https://doi.org/10.1002/adom.201200017

[7] Granqvist, C. G. (2017). Spectrally selective surface coatings for energy efficiency and solar applications, *372*(1984). https://doi.org/10.1119/1.2341584

[8] Yang, S. M., Jang, S. G., Choi, D. G., Kim, S., & Yu, H. K. (2006). Nanomachining by colloidal lithography. *Small*. https://doi.org/10.1002/smll.200500390

[9] Zhang, G., & Wang, D. (2009). Colloidal lithography - The art of nanochemical patterning. *Chemistry - An Asian Journal*. https://doi.org/10.1002/asia.200800298

[10] Inzel, E. D. C. K. (2016). Polycrystalline metasurface perfect absorbers fabricated using microsphere photolithography, 41(15), 3399–3402.

[11] Bonakdar, A., Rezaei, M., Dexheimer, E., & Mohseni, H. (2016). High-throughput realization of an infrared selective absorber / emitter by DUV microsphere projection lithography. *Nanotechnology*, 27, 035301

[12] Ansoft Corporation.Ansoft High Frequency Structure Simulator v10 User guide.2005

[13] " Scattering parameters" Wikipedia. (n.d.).Wikimedia Foundation. Web.

[14] David F. Edwards (1997). *Handbook of Optical Constants of Solids*

[15] Michael Modes (2013). Ther*mal radiation heat transfer*.